Electron-Phonon Coupling in the Bulk of Anatase TiO_2 Measured by Resonant Inelastic X-Ray Spectroscopy

S. Moser,[1,*] S. Fatale,[1] P. Krüger,[2] H. Berger,[1] P. Bugnon,[1] A. Magrez,[1] H. Niwa,[3,4] J. Miyawaki,[3,4] Y. Harada,[3,4] and M. Grioni[1]

[1]*Ecole Polytechnique Fédérale de Lausanne (EPFL), Institut de Physique des Nanostructures, CH-1015 Lausanne, Switzerland*
[2]*Graduate School of Advanced Integration Science, Chiba University, 1-33 Yayoi-cho, Inage, Chiba 263-8522, Japan*
[3]*Institute for Solid State Physics (ISSP), University of Tokyo, Kashiwanoha, Kashiwa, Chiba 277-8526, Japan*
[4]*Synchrotron Radiation Research Organization, University of Tokyo, Sayo-cho, Sayo, Hyogo 679-5198, Japan*

(Received 26 March 2015; published 27 August 2015)

We investigate the polaronic ground state of anatase TiO_2 by bulk-sensitive resonant inelastic x-ray spectroscopy (RIXS) at the Ti L_3 edge. We find that the formation of the polaron cloud involves a single 95 meV phonon along the c axis, in addition to the 108 meV ab-plane mode previously identified by photoemission. The coupling strength to both modes is the same within error bars, and it is unaffected by the carrier density. These data establish RIXS as a directional bulk-sensitive probe of electron-phonon coupling in solids.

DOI: 10.1103/PhysRevLett.115.096404 PACS numbers: 71.38.-k, 78.70.Ck

The microscopic properties of polar semiconductors, such as the lifetime and the effective mass of the charge carriers, are shaped by the electron-phonon (e-ph) interaction. A typical example is that of TiO_2, an important material for photocatalysis [1–3], photovoltaics [4–6], and transparent conductive panels [7]. Angle resolved photoemission (ARPES) results on the anatase polymorph have shown that intermediate-strength coupling to a longitudinal optical (LO) phonon mode determines the nature of the electronic states [8,9]. So-called large polarons are formed, i.e., electrons that coherently propagate with a lattice distortion, with three-dimensional dispersion and a renormalized effective mass in the ab plane $\sim$1.7 times the band mass. ARPES, however, is a surface-sensitive probe, and these conclusions cannot be directly extended to the bulk. In particular, the dielectric environment of TiO_2 may suggest directional screening and, therefore, anisotropic e-ph coupling to a large number of phonon modes [10,11]. As a result, the mass renormalization could be anisotropic, with direct consequences for applications involving transport.

In this Letter we address the bulk e-ph coupling in anatase by resonant inelastic x-ray scattering (RIXS) at the Ti L_3 ($2p \rightarrow 3d$) edge. RIXS is a bulk-sensitive probe of the electronic structure, endowed with chemical and orbital selectivity [12,13]. While its most straightforward application concerns electron-hole excitations, recent work, mainly on cuprate materials, has demonstrated that it can be used to map the dispersion of collective spin excitations [14]. RIXS studies of phonons are less abundant. Measurements on molecules [15] and on cuprates [16,17] have shown that the strength of the e-ph coupling can be extracted from an analysis of the spectral line shape [18]. Our data for anatase exhibit a progression of phonon satellites, corresponding to a LO phonon mode of A_{2u} symmetry which propagates along the c axis. This mode was not captured by a previous ARPES experiment [8], which instead revealed a mode of E_u symmetry, propagating in the perpendicular ab plane. A simple model of e-ph coupling yields for both modes a similar characteristic energy, $\sim$130 meV, in the intermediate-coupling range. These results show that two distinct, highly directional phonon channels along the inequivalent crystal axes of anatase are involved in the formation of the large polaron. Furthermore, the e-ph coupling strength is insensitive to a change of 2 orders of magnitude of the carrier density.

The experiment was performed at beam line BL07LSU of SPring-8. The scattering angle was 90°, the energy resolution was $\sim$100 meV, and the sample temperature $T <$ 40 K [19]. Unless otherwise noted, light was π polarized in the (100) scattering plane, entering the sample at an angle $\alpha = 68°$ with respect to the (001) surface normal (inset, Fig. 1). The transferred moment was $\boldsymbol{q} \sim (0.15\pi/a, 0, 0.92\pi/c)$. All RIXS spectra were normalized to photon flux and acquisition time. A small self-absorption correction was also applied [20].

The left side of Fig. 1 shows the L_3 x-ray absorption (XAS) spectrum of anatase, and a multichannel multiple scattering calculation (MCMS) [22]. The right side of the figure shows RIXS spectra measured at selected photon energies $h\nu$. The RIXS spectra corresponding to XAS features $A1$, $A2$, and $A3$ exhibit symmetric, resolution limited elastic line shapes (pink curve, inset). At XAS feature $B1$, the spectral signature of dd excitations (see below), appears at ~ -1.2 eV and drifts linearly away from the elastic line as $h\nu$ increases from $B1$ to $B2$. In the same range of incident energies, the elastic peak develops an asymmetric tail (blue curve, inset). The coexistence of the dd feature and of the quasielastic tail indicates a close

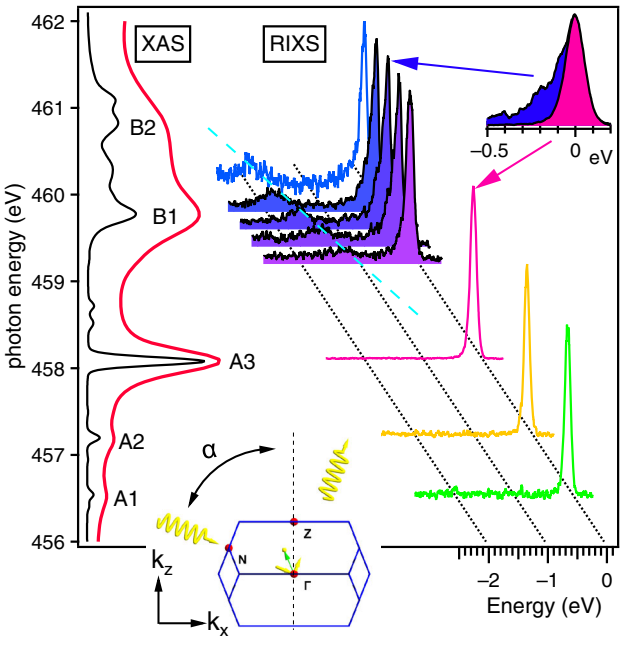

FIG. 1 (color online). (Left) Measured (red line) and calculated (black line) Ti L_3 XAS spectrum of anatase. (Right) RIXS data obtained at different photon energies. The middle inset depicts the experimental geometry with respect to the (100)-projected bulk Brillouin zone. The green arrow represents the transferred momentum $\boldsymbol{q}$.

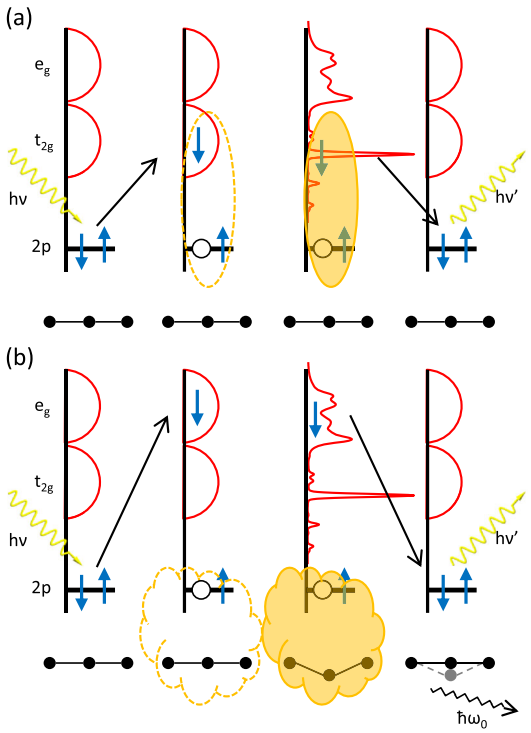

FIG. 2 (color online). (a) Ti L_3 RIXS via a t_{2g} intermediate state. The core hole is well screened by the excited electron. (b) RIXS via an e_g intermediate state. The excited electron is partially delocalized. The poorly screened core hole charge gives rise to a lattice distortion. In the deexcitation process, phonons are emitted.

relation to the orbital nature of the XAS final states $B1$ and $B2$. The $A1$, $A2$, and $A3$ XAS peaks correspond to transitions to t_{2g} crystal field orbitals. According to the MCMS calculation, they have a strongly excitonic character and are intrinsically sharp. By contrast, the $B1$ and $B2$ peaks, which correspond to the more delocalized e_g states, have a finite bandwidth.

The nature—localized vs delocalized—of the intermediate states has direct consequences for the corresponding RIXS signal expressed by [12,13]

$$I(\nu,\nu') = \sum_f \left| \sum_i \frac{\langle f|\hat{\boldsymbol{T}}_2|i\rangle\langle i|\hat{\boldsymbol{T}}_1|g\rangle}{E_i - E_g - h\nu - i\Gamma_i} \right|^2 \times \delta(h\nu - h\nu' + E_g - E_f).$$

$\hat{\boldsymbol{T}}_{1,2}$ is the dipole operator, $|g\rangle$, $|i\rangle$, and $|f\rangle$ are the ground, the intermediate, and the final state in the RIXS process and E_g, E_i, and E_f their corresponding energies; $h\nu$ ($h\nu'$) is the energy of the incident (scattered) light. Figure 2 illustrates schematically two different contributions to the RIXS signal. In Fig. 2(a), the $2p$ electron is excited into a t_{2g} state. The strong Coulomb interaction binds it to the core hole, forming a core exciton. The core hole therefore is well screened and the positive ion cores are unaffected. In Fig. 2(b), the electron is excited into the more delocalized e_g states. The core hole is screened less effectively, and the lattice is locally distorted [see also Fig. 3(c)]. When the core hole is filled in the subsequent deexcitation process, the ions start to oscillate, and the lattice is left in an excited vibrational state. Similar to the Franck-Condon effect in molecules, this produces a sequence of phonon satellites in RIXS, which give rise to the asymmetric tail of the elastic peak.

Unavoidable oxygen vacancies in TiO_2 induce Ti^{3+} sites and dope carriers into the bottom of the conduction band. More vacancies are created by the interaction with the x rays. The number of vacancies, and the corresponding conduction electron density n, can be tuned by adjusting the residual oxygen pressure [8]. Figure 3(a) shows spectra measured at $B1$ ($h\nu = 459.6$ eV) with (blue lines, $n \sim 10^{18}$) and without (red lines, $n \sim 10^{20}$) exposure to an oxygen partial pressure of 2×10^{-5} Pa. The dashed lines are the measured spectra. The solid lines are difference spectra obtained by subtracting the elastic peak (a Voigt fit to the pink curve in Fig. 1) to enhance the visibility of the phonon contributions, which are compared further below (cf). A "one-phonon" line I_1 is observed at $\hbar\omega_0 \sim 95$ meV, followed by two satellites I_2 and I_3, successively separated by $\hbar\omega_0$. The similar line shapes demonstrate that the vibronic excitations are remarkably insensitive to the carrier density [8]. Data measured in specular geometry ($\alpha = 45°$) where $\boldsymbol{q} \sim (0, 0, \pi/c)$ and the momentum

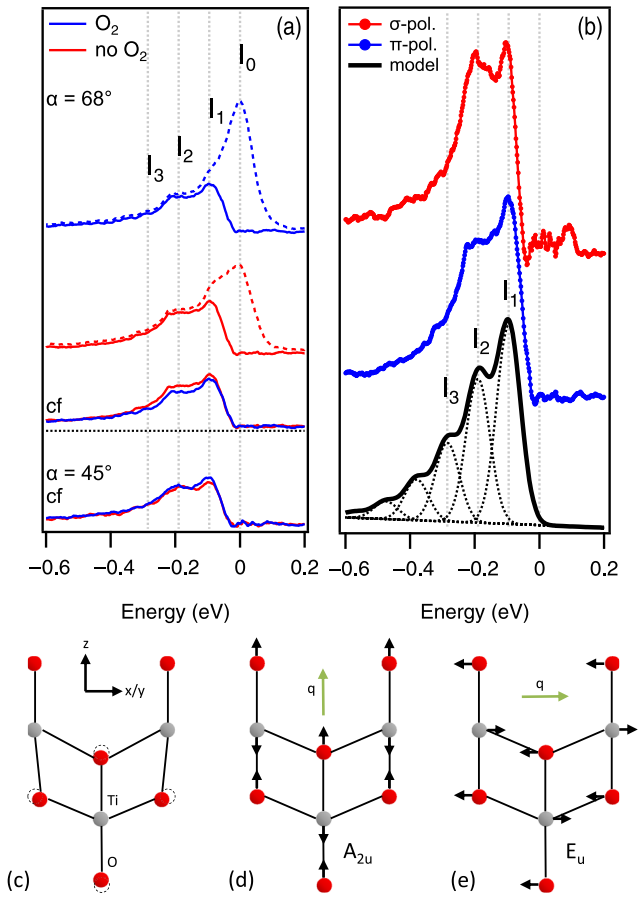

FIG. 3 (color online). (a) RIXS data ($h\nu = 459.6$ eV; π polarization; $\alpha = 68°$) with (blue dashed lines) and without (red dashed lines) oxygen partial pressure. The phonon contributions (solid lines) are compared after subtraction of the elastic peak (cf). A similar comparison is shown for $\alpha = 45°$. (b) Phonon line shapes for σ and π polarization are compared to a model calculation with $\hbar\omega_0 = 95$ meV and $\Gamma = 375$ meV [18]. (c) Cartoon of locally distorted anatase. Schematic displacement patterns for (d) the A_{2u} c-axis phonon, and (e) the E_u in-plane phonon.

transfer within the (001) plane is zero, also exhibit an essentially identical line shape.

The point group symmetry of anatase is D_{4h}. Since the d shell is formally empty, the symmetry of the ground state is A_{1g}. In our experimental geometry with π-polarized light, the dipole operator T^{π} is parallel to the (100) scattering plane yz and described by irreducible representations E_u and A_{2u}. The dipole allowed intermediate states are thus contained in $A_{1g} \otimes (E_u \oplus A_{2u}) = E_u \oplus A_{2u}$. Since the absorption is local at a Ti site, inversion symmetry is lost and the intermediate states branch to $E \oplus B_2$ in point group D_{2d}. For the deexcitation process, we apply the dipole operator in D_{2d} and obtain $(E \oplus B_2) \otimes (E \oplus B_2) = A_1 \oplus A_2 \oplus B_1 \oplus B_2 \oplus E$. In σ polarization, T^{σ} is only contained in the E_u irreducible representation of D_{4h} and the dipole allowed final states do not contain the E modes. Because of the loss of inversion symmetry in the intermediate state, both even and odd RIXS final states are accessible [23].

Figure 3(b) shows two representative phonon spectra measured with π and σ polarization. Their similar line shapes imply a negligible contribution of the E branch to the phonon shoulder. Among the remaining branches, Raman [24,25] and optical reflectivity measurements [26] have identified A_{1g} (63.6 meV), B_{1g} (64.3 meV), and A_{2u} (93.6 meV) modes. A good agreement with the data is found for the latter, a LO phonon involving opposite atomic displacements of Ti and O ions along the c axis, sketched in Fig. 3(d) [26]. First-principles calculations [27,28] find this phonon branch to be real valued and weakly dispersing only along the ΓZ high symmetry direction of the 3D Brillouin zone. This is an interesting observation since ARPES data [8] reveal instead a single ab-plane infrared active LO E_u phonon mode of energy $\hbar\omega_{E_u} \sim 108$ meV [26], sketched in Fig. 3(e). Nevertheless, the ARPES and RIXS data are not contradictory but are complementary. Our RIXS experiment, which mostly probes momentum transfer along the c axis, is insensitive to the ab-plane mode. On the other hand, a component at 95 meV would be compatible with the line width of the ARPES spectral features. Therefore, the combined ARPES and RIXS data indicate that the polarization cloud of the large polaron is built from the coherent superposition of well-defined in-plane and c-axis optical modes, with similar displacement patterns and slightly different energies, reflecting the anisotropy of the elastic properties of anatase.

To assess the coupling strength to the A_{2u} phonon, we start with the Fröhlich Hamiltonian:

$$H = M\sum_R d_R^{\dagger} d_R (b_R^{\dagger} + b_R) + \hbar\omega_0 \sum_R b_R^{\dagger} b_R, \qquad (1)$$

with one LO Einstein phonon mode $\hbar\omega_0$ and e-ph coupling energy M. $d^{\dagger}$ (d) and $b^{\dagger}$ (b) are, respectively, electron and phonon creation (annihilation) operators. The RIXS intensity of the nth phonon satellite can be calculated analytically [18]:

$$I(h\nu, h\nu') \propto \left| \sum_{n'=0}^{\infty} \frac{B_{\max(n,n'),\min(n',n)}(g) B_{n',0}(g)}{(g - n')\hbar\omega_0 + i\Gamma} \right|^2. \qquad (2)$$

$g = M^2/(\hbar\omega_0)^2$ is the dimensionless e-ph coupling strength and $B_{m,n}(g)$ are Franck-Condon factors. The calculated spectrum for $\hbar\omega_0 = 95$ meV and lifetime $\Gamma = 375$ meV, estimated from photoemission [20], is shown in Fig. 3(b). The best fit to the data is obtained for an e-ph coupling energy $M = 130$ meV. Alternatively, M can be estimated from the intensity ratio of the two- and one-phonon satellites: $I_2/I_1 = M^2/\Gamma^4$. The value $I_2/I_1 = 0.86 \pm 0.08$ extracted from the spectra for both polarizations again yields $M = 130 \pm 6$ meV. The corresponding coupling parameter $g \sim 1.89 \pm 0.16$ is consistent with

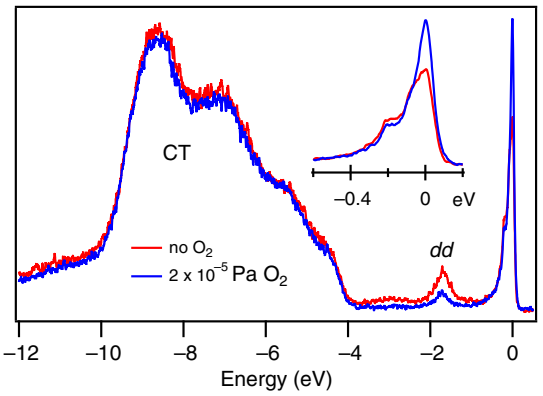

FIG. 4 (color online). RIXS data taken with $h\nu = 459.6$ eV and π-polarized light with (blue lines) and without (red lines) an oxygen partial pressure. In contrast to the charge transfer (CT) excitations and the phonon shoulder (inset), oxidation leads to a larger elastic line but a lower *dd* peak.

the surface-sensitive ARPES estimate [8] and places anatase in the intermediate-coupling regime.

Finally, we address the *dd* excitations. Stoichiometric anatase TiO_2 is formally a d^0 system and *dd* electronic transitions are not possible. However, as already discussed, oxygen vacancies dope carriers into the bottom of the t_{2g}-derived conduction band [8]. New *dd* loss processes are now allowed when the RIXS excitation is into the e_g manifold, but the deexcitation comes from a t_{2g} band [29,30]. Their signature is the non-Raman peak around −1.7 eV. Sample reoxidation depletes the conduction band and reduces the intensity of this channel relative to (quasi-) elastic scattering. Figure 4 shows the spectra of Fig. 3 over a broader energy range. The dominant charge transfer (CT) feature remains unaffected by oxygen exposure. By contrast, the elastic line is enhanced while the *dd* intensity is reduced, consistent with the previous argument.

To summarize, these RIXS results conclusively establish the importance of *e*-ph coupling in the bulk of anatase TiO_2. We find that the polaronic cloud is built from distinct phonon modes with slightly different energies: an in-plane E_u and a *c*-axis A_{2u} phonon. The data further show that the *e*-ph interaction strength and the resulting phonon renormalization of the charge carriers are essentially isotropic, and they are unaffected by a 2 orders of magnitude change of the conduction electron density.

With the expected order-of-magnitude improvement of energy resolution in the new generation of instruments now under construction, RIXS will become an even more powerful direct and selective probe of *e*-ph coupling. The improved resolution will, namely, make it possible to disentangle phonon and magnon contributions that partially overlap in the *L*-edge spectra of cuprate materials and limit, at present, the accuracy of the analysis [31]. At transition metal *K* edges, in the hard x-ray range, orbital selectivity can be further increased, taking advantage of the absence of spin-orbit and of smaller multiplet effects [16]. Moreover, compared to nonresonant scattering techniques, the high sensitivity of RIXS will enable measurements of small sample volumes like interfaces or thin films, thus providing access to a variety of technologically relevant materials.

This work was carried out under Proposal No. 2013B7455 at SPring-8. We gratefully acknowledge valuable discussions with D. Malterre, R. Claessen, A. Santander-Syro and L. Österlund, and financial support by the Swiss National Science Foundation and by the Photon and Quantum Basic Research Coordinated Development Program from MEXT, Japan.

*simon.moser@epfl.ch

[1] R. Asahi, T. Morikawa, T. Ohwaki, K. Aoki, and Y. Taga, Science **293**, 269 (2001).
[2] Y. He, A. Tilocca, O. Dulub, A. Selloni, and U. Diebold, Nat. Mater. **8**, 585 (2009).
[3] A. Fujishima and K. Honda, Nature (London) **238**, 37 (1972).
[4] B. O'Regan and M. Grätzel, Nature (London) **353**, 737 (1991).
[5] D. Kuang, J. Brillet, P. Chen, M. Takata, S. Uchida, H. Miura, K. Sumioka, S. M. Zakeeruddin, and M. Grätzel, ACS Nano **2**, 1113 (2008).
[6] O. K. Varghese, M. Paulose, and C. A. Grimes, Nat. Nanotechnol. **4**, 592 (2009).
[7] T. Hitosugi, Y. Furubayashi, A. Ueda, K. Itabashi, K. Inaba, Y. Hirose, G. Kinoda, Y. Yamamoto, T. Shimada, and T. Hasegawa, Jpn. J. Appl. Phys. **44**, 34 (2005).
[8] S. Moser, L. Moreschini, J. Jaćimović, O. S. Barišić, H. Berger, A. Magrez, Y. J. Chang, K. S. Kim, A. Bostwick, E. Rotenberg, L. Forró, and M. Grioni, Phys. Rev. Lett. **110**, 196403 (2013).
[9] M. Setvin, C. Franchini, X. Hao, M. Schmid, A. Janotti, M. Kaltak, C. G. Van de Walle, G. Kresse, and U. Diebold, Phys. Rev. Lett. **113**, 086402 (2014).
[10] C. Persson and A. Ferreira da Silva, Appl. Phys. Lett. **86**, 231912 (2005).
[11] J. P. Hague, P. E. Kornilovitch, A. S. Alexandrov, and J. H. Samson, Phys. Rev. B **73**, 054303 (2006).
[12] A. Kotani and S. Shin, Rev. Mod. Phys. **73**, 203 (2001).
[13] L. J. P. Ament, M. van Veenendaal, T. P. Devereaux, J. P. Hill, and J. van den Brink, Rev. Mod. Phys. **83**, 705 (2011).
[14] M. P. M. Dean, J. Magn. Magn. Mater. **376**, 3 (2015).
[15] F. Hennies, A. Pietzsch, M. Berglund, A. Föhlisch, T. Schmitt, V. Strocov, H. O. Karlsson, J. Andersson, and J.-E. Rubensson, Phys. Rev. Lett. **104**, 193002 (2010).
[16] H. Yavaş, M. van Veenendaal, J. van den Brink, L. J. P. Ament, A. Alatas, B. M. Leu, M.-O. Apostu, N.Wizent, G. Behr, W. Sturhahn, H. Sinn, and E. E. Alp, J. Phys. Condens. Matter **22**, 485601 (2010).
[17] W. S. Lee, S. Johnston, B. Moritz, J. Lee, M. Yi, K. J. Zhou, T. Schmitt, L. Patthey, V. Strocov, K. Kudo, Y. Koike, J. van den Brink, T. P. Devereaux, and Z. X. Shen, Phys. Rev. Lett. **110**, 265502 (2013).
[18] L. J. P. Ament, M. van Veenendaal, and J. van den Brink, Europhys. Lett. **95**, 27008 (2011).

[19] Y. Harada, M. Kobayashi, H. Niwa, Y. Senba, H. Ohashi, T. Tokushima, Y. Horikawa, S. Shin, and M. Oshima, Rev. Sci. Instrum. **83**, 013116 (2012).
[20] See Supplemental Material at http://link.aps.org/supplemental/10.1103/PhysRevLett.115.096404, which includes Ref. [21], for sample preparation, self-absorption, and lifetime estimation of the intermediate state.
[21] H. Berger, H. Tang, and F. Lévy, J. Cryst. Growth **130**, 108 (1993).
[22] P. Krüger, Phys. Rev. B **81**, 125121 (2010).
[23] M. Tinkham, *Group Theory and Quantum Mechanics* (McGraw-Hill, New York, 1964).
[24] T. Ohsaka, F. Izumi, and Y. Fujiki, J. Raman Spectrosc. **7**, 321 (1978).
[25] Z.-G. Mei, Y. Wang, S.-L. Shang, and Z.-K. Liu, Inorg. Chem. **50**, 6996 (2011).
[26] R. J. Gonzalez, R. Zallen, and H. Berger, Phys. Rev. B **55**, 7014 (1997).
[27] M. Mikami, S. Nakamura, O. Kitao, and H. Arakawa, Phys. Rev. B **66**, 155213 (2002).
[28] E Shojaee and M. R. Mohammadizadeh, J. Phys. Condens. Matter **22**, 015401 (2010).
[29] A. Augustsson, A. Henningsson, S. M. Butorin, H. Siegbahn, J. Nordgren, and J.-H. Guo, J. Chem. Phys. **119**, 3983 (2003).
[30] K.-J. Zhou, M. Radovic, J. Schlappa, V. Strocov, R. Frison, J. Mesot, L. Patthey, and T. Schmitt, Phys. Rev. B **83**, 201402(R) (2011).
[31] M. Guarise *et al.*, Phys. Rev. Lett. **105**, 157006 (2010).